Original

Preparation of glass–ceramic materials from coal ash and rice husk ash: Microstructural, physical and mechanical properties

Julián Dávalos[a], Ashley Bonilla[a], Mónica A. Villaquirán-Caicedo[a],,
Ruby M. de Gutiérrez[a], Jesús Ma. Rincón[b]*

[a] *Composite Materials Group (CENM), School of Materials Engineering, University of Valle, Calle 13 No.100-00, Cali, Colombia*
[b] *Eduardo Torroja Institute for Construction Science, Glassy and Ceramic Materials Laboratory, CSIC, c/ Serrano Galvache 4, 28033 Madrid, Spain*

ABSTRACT

Wastes such as coal and rice husk ashes, which are widely available in Colombia, were successfully used to synthesize glass-ceramics in the (Na_2O)–CaO–Al_2O_3–SiO_2 system, which are obtained from thermally treating the parent glasses. The raw materials were mechanically conditioned, and the glasses were designed based on the CaO/SiO_2 molar ratio, which was varied between 0.25 and 0.39. The glasses were obtained by melting the powders at 1450 °C for 2 h, and the melted powder was then poured into water. To obtain the glass–ceramic material, the temperature of the glass thermal treatment, which was generally lower than 1000 °C in all cases, was determined by differential thermal analysis. The glass-ceramics obtained were microstructurally, physically and mechanically characterized. In addition, the durability was determined in acidic and alkaline environments (HCl and NaOH solutions). Glass–ceramics with densities of 2607–2739 kg/m³, water absorption below 0.1%, Vickers hardness above 600 MPa and elastic modulus of ∼96 GPa were obtained. The fracture toughness K_{ic} was in the range of 0.39–0.59 MPa m$^{1/2}$. The chemical durability was considered excellent (with mass losses of ∼0.5 mg/cm²), therefore these glass–ceramics can be good candidates for different applications in the construction sector.

Preparación de vitrocerámicas a partir de ceniza de carbón y ceniza de cascarilla de arroz: microestructura, propiedades físicas y mecánicas

RESUMEN

Residuos sólidos como ceniza de carbón y ceniza de cascarilla de arroz, los cuales se encuentran disponibles en grandes cantidades en Colombia, se emplearon para la síntesis (a partir de vidrios parental) de materiales vitrocerámicos dentro del sistema SiO_2–Al_2O_3–$CaO(Na_2O)$.

* Corresponding author.
  E-mail address: monica.villaquiran@correounivalle.edu.co (M.A. Villaquirán-Caicedo).

Ceniza de cáscara de arroz
Ceniza de carbón
Microestructura
Propiedades mecánicas

Las materias primas se acondicionaron mecánicamente y los vidrios se diseñaron basados en la relación molar CaO/SiO$_2$, la cual varió entre 0,25 y 0,29. Los vidrios se obtuvieron por fusión a 1.450 °C por 2 h y el material fundido se enfrió en agua. Para obtener la vitrocerámica, el vidrio fue analizado por análisis térmico diferencial para identificar la temperatura de cristalización, que fue menor de 1.000 °C para todos los vidrios en estudio. Las vitrocerámicas obtenidas fueron caracterizadas microestructural, física y mecánicamente. Además, la durabilidad fue determinada en ambiente ácidos y básicos en soluciones de HCl y NaOH. Se obtuvieron vitrocerámicas con densidades entre 2.607 y 2.739 kg/m^3, con absorción de agua menor al 0,1%, dureza Vickers de 600 MPa y módulo de elasticidad de ∼96 GPa. La tenacidad a la fractura K_{ic} estuvo en el rango de 0,39-0,59 MPa m$^{1/2}$ y la durabilidad química fue considerada como muy buena debido a las pérdidas de masa de tan solo ∼0,5 mg/cm^2. Con estos resultados, las vitrocerámicas obtenidas se consideran buenas candidatas para aplicaciones en el sector de la construcción.

Introduction

Glass–ceramics are ceramic materials formed through the controlled nucleation and crystallization of glass, generally induced by nucleating additives [1,2]. They always contain a residual glassy phase and one or more embedded crystalline phases [2–4]. Others glass–ceramics can be obtained without the addition of nucleating agents [5,6] giving rise to excellent properties. Some of the most important properties of glass–ceramics are their high strength and toughness, they have zero or very low porosity, thermal stability and chemical durability [2]. Due to their wide range of properties, glass–ceramics have been studied in recent years for different applications, for example, as materials for the dental implants [7]; luminescent materials based on Eu^{3+}-doped aluminosilicates [8], and rare-earth-free glass–ceramic-based phosphor [9]; high-temperature resistant materials (1200 °C) based on anorthite and tialite [10]; glass–ceramic with improves mechanical properties as high micro-hardness, high flexural strength and low friction coefficient [11]; dielectric materials prepared at ultralow temperatures using alumina, quartz and zirconium [12]; dielectric materials based on albite structures [13]; glass–ceramics containing 40% or more ZnO for wastewater decontamination via photocatalysis [14]; materials for waste vitrification [4], among others.

Glass–ceramics as vitrification and devitrification process has been used to neutralize different potentially dangerous industrial wastes [15–17], and to stabilize and reduce the volume of wastes by between 20% and 97% depending on their nature [17,18]. In addition, to reducing waste volume, the devitrification process increases the added-value and reduces the environmental impact of different inorganic wastes [4]. Industrial aluminosilicate wastes and byproducts, which include blast furnace slag, fly ash and ashes from other industrial processes [17–22] have been investigated for their use as raw materials to produce glass–ceramics. Recent studies have used ash obtained from incinerating municipal wastes to replace the conventional clays used to synthesize glass–ceramics by taking advantage of its ability to immobilize heavy metals; wastes of incinerator ashes have been mixed with marble sludge to obtain materials with mechanical properties similar to those of commercial glass–ceramics [23]. Other agricultural wastes with a high content of SiO$_2$, such as rice husk ash (RHA), whose annual generation is approximately 132 Mt [24], can also be used as raw materials to produce glass–ceramics. The different properties of the glass–ceramic materials obtained from RHA can be used for a wide range of applications. Wang [20] and Zhu [17] produced glass–ceramic foams that can be used as thermal insulators; the authors reported compressive strengths of 9.84 MPa and above 5 MPa for materials with bulk densities of 0.98 g/cm^3 and 0.46 g/cm^3, respectively. Composite glass–ceramics made with RHA and sugar cane ash have exhibited photoluminescent properties for possible applications in power generation, LEDs and high-temperature applications [25]. In addition, RHA was also used to prepare bioactive glass–ceramic, potentially suitable material for bone reconstruction and tissue engineering applications [26].

In Colombia, industrial wastes such as rice husk or coal ashes are not being used and are disposed of in uncontrolled landfills generating high environmental impact. There is a significant interest in finding applications for the development of value-added products. Therefore, the goal of the present investigation is to produce materials with glass–ceramic characteristics using these industrial wastes. In the first stage, glasses with different CaO/SiO$_2$ molar ratios were designed and produced, and the glass–ceramics were then characterized to determine their physical (density, absorption and porosity) and mechanical (Vickers hardness, Young's modulus and fracture toughness) properties and durability (mass loss after exposure to acids and bases).

Materials and methodology

The methodology followed in the present investigation for obtaining glass–ceramics is summarized in Fig. 1. Raw materials and Design and obtention of glasses and glass–ceramics section explain the process.

Raw materials

The raw materials used to synthesize the original glasses, which were subsequently crystallized to obtain the glass–ceramics, were rice husk ash (RHA), coal ash (CA)
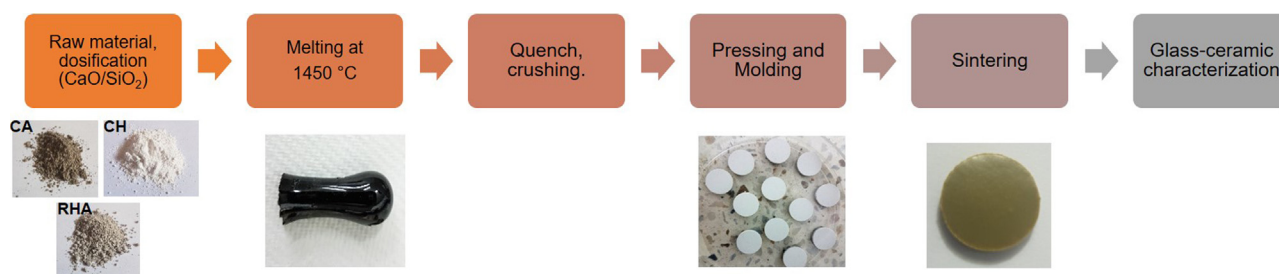
Fig. 1 – Procedure used to prepare coal ash-RHA-based glass–ceramics (CA: coal ash, CH: calcium hydroxide, RHA: rice husk ash).
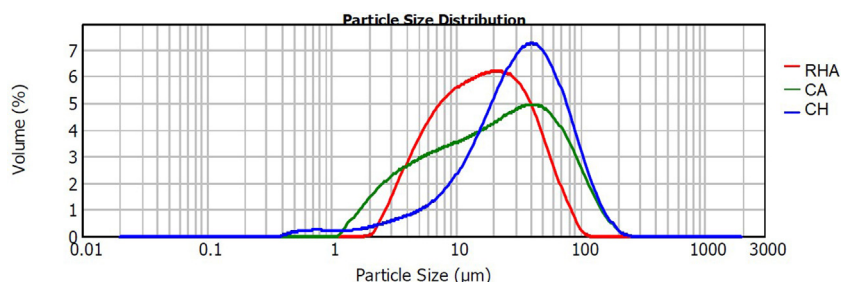

Fig. 2 – Particle size distribution of the raw materials.

and commercial calcium hydroxide ($Ca(OH)_2$=CH) (Fig. 1). The CA was obtained from the furnace of the Lago Verde brick company (southwestern region of Colombia), and the RHA was rice husk that had been burned at 600 °C for 2 h at the La Esmeralda rice company (Jamundi). The CH was commercially acquired (Corona®, Colombia). The starting materials CA and RHA were mechanically conditioned in a US Stoneware ceramic ball mill. The particle size and distribution of the raw materials was determined with a Mastersizer 2000 laser granulometry device (Malvern Instrument), using water as the dispersing medium. The average particle size of the CA, RHA and CH was 33.48, 21.87 and 41.15 μm, respectively, and the particle size distribution can be observed in Fig. 2. The density of the raw materials was determined by following the ASTM C127-04 standard and using the pycnometer method; the density of the CA, RHA and CH was 2480, 2000 and 2250 kg/m³, respectively.

The chemical composition of the CA, RHA and CH, as presented in Table 1, was determined with a PANalytical sequential wavelength dispersive X-ray fluorescence spectrometer (WDXRF), model AXIOS mAX, equipped with a rhodium tube and operated with a maximum power of 4.0 kW, and the SuperQ software version 5.0 L was used. The results show that the CA has an elevated content of SiO_2 and Al_2O_3 (with a SiO_2/Al_2O_3 molar ratio of 4.0), but its alkali level is quite low; the RHA has an elevated content of SiO_2 (95.59 wt%).

The mineralogical composition of the CA was determined using a X'Pert MRD PANalytical diffractometer with CuKα radiation generated at 45 kV and 40 mA; the specimens were scanned between 10 and 60° 2θ with a step size of 0.02°. The X-ray diffraction patterns are shown in Fig. 3, where the presence of traces quartz (*Inorganic Crystal Structure Database*, ICSD 100341) is observed in the RHA. However, the increasing baseline between 18 and 30° 2θ indicates the presence of a large

Table 1 – Chemical composition of the raw materials.			
Component	CH (wt%)	CA (wt%)	RHA (wt%)
SiO_2	0.52	62.13	95.59
Al_2O_3	0.17	26.36	0.19
CaO	71.47	1.27	0.65
Na_2O	0.02	0.27	0.07
Fe_2O_3	0.07	4.88	0.18
K_2O	–	0.81	0.16
MgO	1.81	0.25	0.51
CuO	–	0.01	–
ZnO	–	1.19	–
TiO_2	–	0.01	–
P_2O_5	0.01	–	–
SO_3	0.48	–	–
Cl	0.10	–	–
SrO	0.03	–	–
Loss on ignition (1000 °C)	25.42	1.02	2.66

amount of reactive or amorphous silica. The crystalline phases identified for the CA were quartz (ICSD #100341), hematite (ICSD #066756) and mullite (ICSD #066445).

Design and obtention of glasses and glass–ceramics

The raw materials to produce the glass–ceramics correspond to the (Na_2O)–CaO–Al_2O_3–SiO_2 ternary system shown in Fig. 4a. Highlighted inside the red circle are the crystalline phases that should be obtained according to the raw material used. The material of interest is then a glass–ceramic containing tridymite, anorthite and pseudowollastonite phases, which in principle, could give to the final glass–ceramic to good mechanical properties and a high hardness [1,27]. Anorthite is characterized as having a high chemical resistance in alkaline and acidic environments [27,28]. To comply with the above-mentioned recommendations, five mixtures were designed, in which the CaO/SiO_2 molar ratio was varied between 0.25

ID sample	CA, wt%	RHA, wt%	CH, wt%	CaO/SiO$_2$ molar ratio	SiO$_2$/Al$_2$O$_3$ molar ratio
0.25	30	50	20	0.25	13.74
0.29	60	20	20	0.29	5.98
0.33	30	45	25	0.33	12.76
0.35	40	35	25	0.35	9.15
0.39	60	15	25	0.39	7.54

Table 2 – Mixture design used to obtain the glasses.

Fig. 3 – X-ray diffraction patterns of the raw materials.

Considering the proportion of the mixture components (Table 2), the composition of the designed glasses is presented in Table 3. The parental glasses are identified by the GXX code, and the thermally treated materials (glass–ceramics) are identified by the GCXX code; in both cases, XX represents the CaO/SiO$_2$ molar ratio used in the mixture.

The powders (CA, RHA and CH) were previously homogenized and placed in alumina crucibles (Fisherbrand™), which were then subjected to 1450 °C in a Nabertherm electric furnace; a heating rate of 15 °C/min was used, and the samples were held for 2 h at the maximum temperature to completely melt the powders. The viscous fluid obtained was poured into water to produce the parent glass (G) particles. The G particles were then manually ground in a mortar to thus obtain the glass powders, which were then subsequently sintered. To obtain glass–ceramic with good properties, it is necessary to control the process to crystallize the parent glass by determining the optimum temperature for crystal nucleation and growth, by differential thermal analysis. This technique can be used to identify the exothermic crystallization peak (T_c). Once the crystallization temperatures are identified, the parental glass powders are compacted into circular pellets with 13 mm diameters (approximately 0.5 g of material). A 10% wt H$_2$O solution was used as the binder for compaction, which was performed with a manual press (CrushIR, Pike Technologies) operated with a pressure between 8 and 9 tons. After powder compaction, the samples were stored in a desiccator to prevent the inclusion of moisture. Then, the pellets were heating up in one-step until Tc, and maintained during 2 h at this temperature. After the glass–ceramics obtained were characterized.
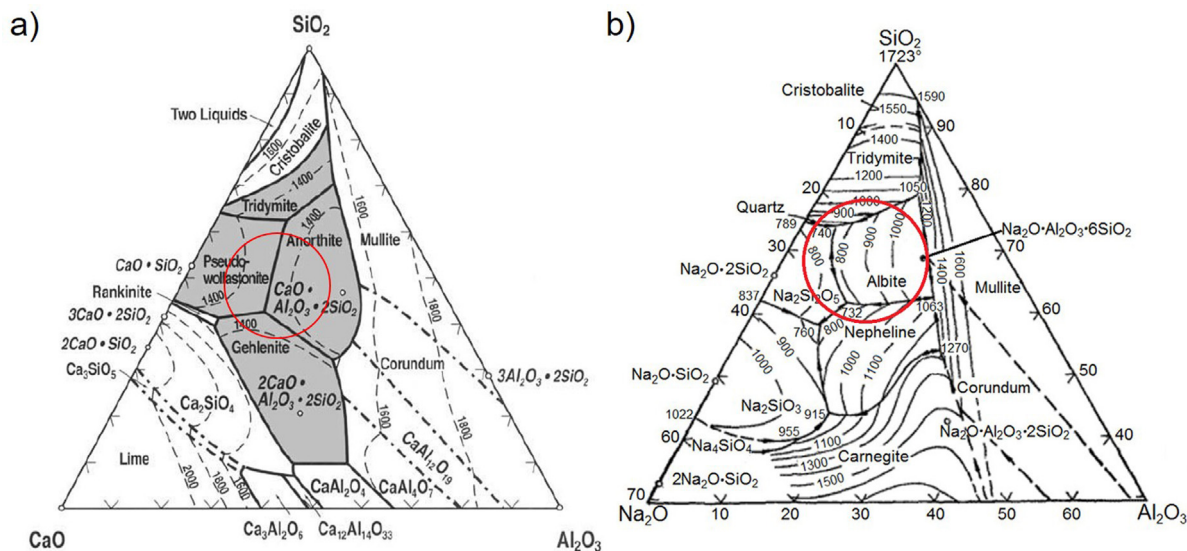
and 0.39 (Table 2). To synthesize the glass, a powder mixture was prepared comprising 90 wt% of the raw materials (according to Table 2), 5 wt% of the network modifier (ZnO) and 5 wt% of sodium tetraborate (Na$_2$B$_4$O$_7$), which acts as the fluxing agent and decreases the viscosity of the molted material [29]. Due to incorporating the fluxing agent, it is possible after the sintering processes to form sodium-rich crystalline phases, as observed in the Na$_2$O–Al$_2$O$_3$–SiO$_2$ diagram (Fig. 3b).

Fig. 4 – (a) Ternary SiO$_2$–Al$_2$O$_3$–CaO diagram [1]. (b) SiO$_2$–Al$_2$O$_3$–Na$_2$O diagram [30].

Table 3 – Chemical compositions of the designed glasses.						
Glass ID	SiO$_2$, wt%	Al$_2$O$_3$, wt%	CaO, wt%	Na$_2$O, wt%	K$_2$O, wt%	ZnO, wt%	Fe$_2$O$_3$, wt%
G0.25	64.91	8.02	14.99	5.11	0.24	5.0	1.46
G0.29	55.85	15.86	15.18	5.19	0.49	5.0	2.93
G0.33	60.32	8.02	18.53	5.11	0.24	5.0	1.46
G0.35	57.30	10.63	18.60	5.14	0.32	5.0	1.95
G0.39	51.26	15.86	18.72	5.20	0.49	5.0	2.93

Characterization of parent glasses and glass–ceramics

The following techniques were used:

- The thermal analysis test (Differential Scanning Calorimetry) was performed with a TA Instruments STD Q-600 device operated with a nitrogen atmosphere, temperature range of 40–950 °C, heating rate of 10 °C/min and N$_2$ flow of 100 ml/min.
- Scanning electron microscopy (SEM) was used to evaluate the microstructure. This test was performed with a JEOL JSM-6490LV instrument using the backscattered electron method. To observe the thermally treated samples (glass–ceramics), the surface was previously attacked with 5% hydrofluoric acid (HF), which dilutes the amorphous portion and allows the sample microstructure to be observed. Then, the samples were surface coated with gold for 15 s using Denton Vacuum equipment (Model Desk IV) to achieve a conducting surface.
- The apparent density, percentage of absorption and volume of permeable voids were determined according to a slight modification of the ASTM C642 standard, in which the samples were immersed in water at 100 °C for 2 h instead of the 5 h specified in the standard for Portland cement-based materials. Two samples for every composition were evaluated.
- Solutions of NaOH and HCl with concentrations of 0.01 M were prepared for the chemical resistance test. The test was performed based on the methodology used by Zhang et al. [29], which consists on introducing the pellets into these solutions at 95 °C for 6 h and monitoring the mass loss every 2 h. Two samples for every composition were evaluated.
- The microhardness was evaluated using the Vickers hardness test according to the ASTM C1327-15 standard. The equipment used for this test was a THV-1D digital microhardness tester from Beijing Time High Technology Ltda. The load used was 1 kgF. In addition, the Young's modulus (E) was evaluated by the instrumented nanoindentation test (Hysitron TI950 TriboIndenter, Bruker) with a Berkovich diamond tip and a 5 × 5 matrix. Each consecutive indentation was separated by 4.5 μm to prevent the residual stresses of the adjacent imprints from interfering with each other. The calibration test was performed with fused silica sample with a maximum load 300 mN. The force–displacement curves were used to determine the elastic moduli. The E determined for each indentation was calculated using the standard methods of Oliver and Pharr with Equation 1 given in the [31] reference:

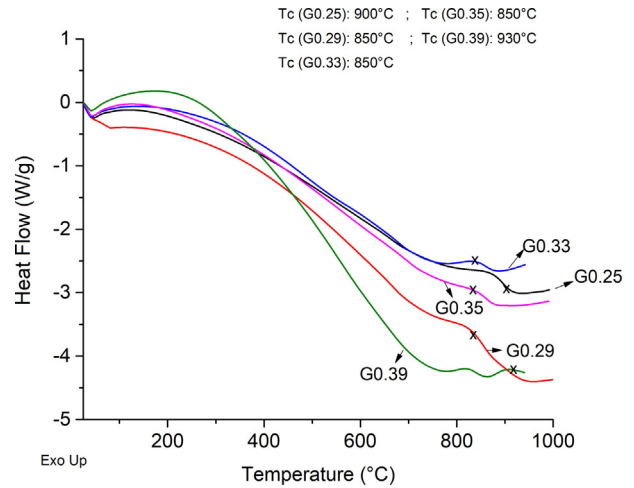$$E = (1 - \nu^2)\left[\frac{1}{E_r} - \frac{\nu_i^2}{E_i}\right]^{-1} \quad (1)$$

Fig. 5 – DSC curves obtained for the glasses, was used to determine the T_c. The select T_c is marked with (x).

where ν corresponds to the Poisson's ratio, estimated to be 0.245 for a glass–ceramic of the CaO–SiO$_2$–Al$_2$O$_3$ system [32], E_r (GPa) corresponds to the reduced modulus of the studied glass–ceramics, and ν_i (0.07) and E_i (1141 GPa) are the data associated with the Berkovich indenter. The applied load was in the unloading mode from 10,000 μN down to 160 μN. The hardness values (H) were calculated by following the procedure of Oliver and Pharr, and therefore, these values correspond to the averages obtained for each group of indentations. The fracture toughness (K_{ic}) was calculated using the model of Anstis et al. [33] according to Eq. (2), which is based on the measured length of the cracks coming from the corners of the Vickers notches:

$$K_{ic} = 0.016\sqrt{\frac{E}{H}}\left(\frac{P}{c^{3/2}}\right) \quad (2)$$

where P is the load in newtons, c is the crack length from the center of the indent to the crack tip in meters, E is the Young's modulus and H is the Vickers hardness in GPa.

Results and analysis

Microstructure of the ceramics obtained from the glasses with different CaO/SiO$_2$ ratios

The Differential Scanning Calorimetry (DSC) curves of the parent glasses are shown in Fig. 5. Although the DSC tests do not show that the glasses obtained have high devitrification capacities, the crystallization temperature (T_c) for samples
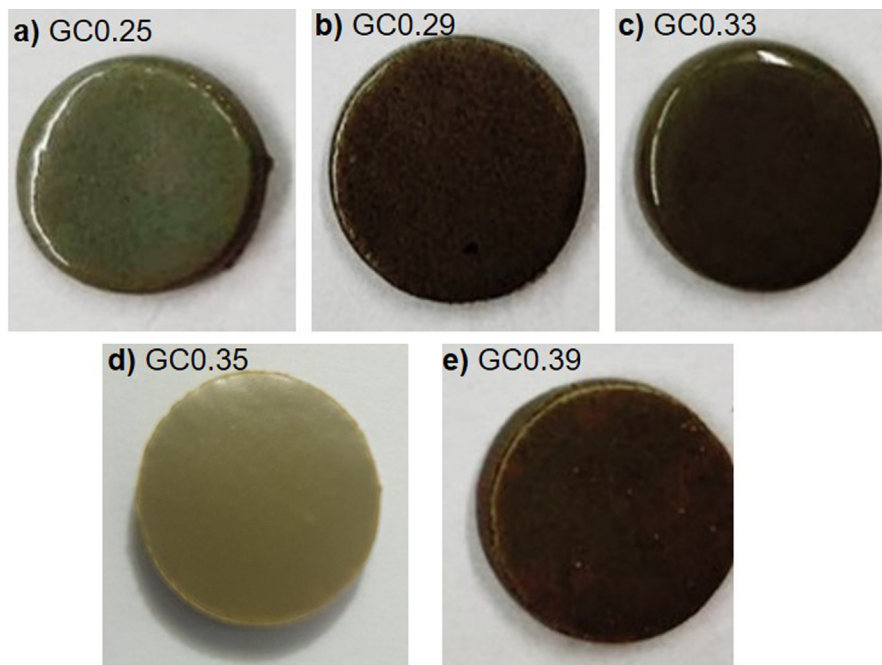
Fig. 6 – Appearance of the sintered samples.

were selected from the obtained graphs. In general, these T_c temperatures range between 850 °C and 930 °C. Fig. 6 shows images of the materials obtained after the sintering processes, where it can be observed that at a higher SiO_2/Al_2O_3 molar ratio, the samples have a brighter appearance and rounded edges, which is due to the low viscosity of the glassy phase. The GC0.35 and GC0.39 samples are appearing opaquer and have well-defined edges, just these samples have high CaO/SiO_2 molar ratio and low SiO_2/Al_2O_3 molar ratio. Note that the samples with glassy appearance correspond to the samples with higher SiO_2/Al_2O_3 molar ratios (Table 2).

The XRD patterns obtained for the sintered samples are shown in Fig. 7. Anorthite ($CaAl_2SiO_2O_8$) and albite ($(Na,Ca)(Si,Al)_4O_8$) are mainly observed to form in the sintered samples GC0.29, GC0.35 and GC0.39, which correspond to the mixtures with lower SiO_2/Al_2O_3 molar ratios (5.98, 9.15 and 5.48, respectively). In contrast, the XRD patterns of the samples GC0.25 and GC0.33, which correspond to the higher SiO_2/Al_2O_3 molar ratios, 13.74 and 12.76, respectively, showed small peaks corresponding to cristobalite (SiO_2) and a higher content of the glassy phase. Notably, wollastonite ($Ca_3Si_3O_9$) was expected to form in these mixtures. The absence of wollastonite can be attributed to the high contents of Al_2O_3 in CA and to the low percentage of CaO present in the mixtures. Soares et al., obtained wollastonite at temperatures of approximately 900 °C but observed higher contents of Ca in the mixture [35]. In conventional sintered glasses, small crystals grow in size, and phases with anorthite or plagioclase crystals are common [27,36]. Therefore, both the CaO/SiO_2 and SiO_2/Al_2O_3 molar ratios affect the formation of the crystalline phases and have to be considered simultaneously in the material design.

The albite crystalline phase is found in the $Na_2O–Al_2O_3–SiO_2$ system, and its formation is due to
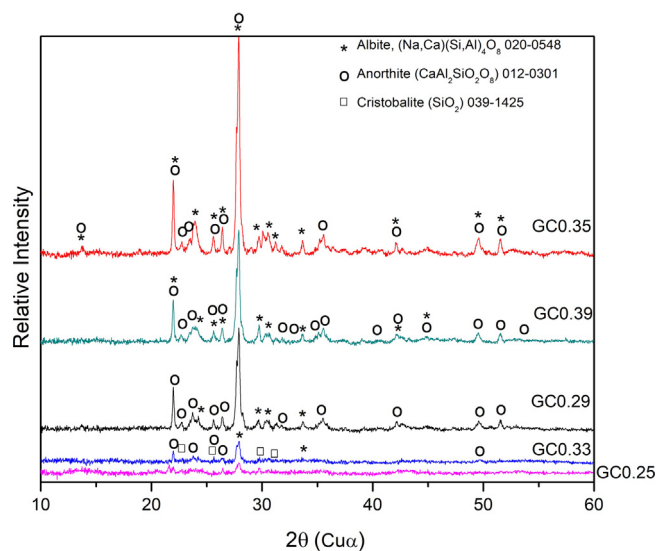

Fig. 7 – X-ray diffraction pattern of the sintered samples.

incorporating Na_2O as a fluxing agent. The sodium atoms are introduced into the silica and alumina tetrahedral structure, which are found in the same region in the $CaO–Al_2O_3–SiO_2$ and $NaO_2–Al_2O_3–SiO_2$ ternary diagrams, as shown in Fig. 4b.

Fig. 8 shows the SEM images of the sintered samples. The presence of the glassy phase is mainly observed in the GC0.25 (Fig. 8a) and GC0.33 (Fig. 8c) samples. The XRD patterns of these samples contained small crystalline peaks associated with traces of cristobalite. For the GC0.29 and GC0.35 samples, the formation of the lamellar anorthite crystals and albite is confirmed by the needle-shape morphology, which has been identified by other authors [27,37]. The glassy phase is also
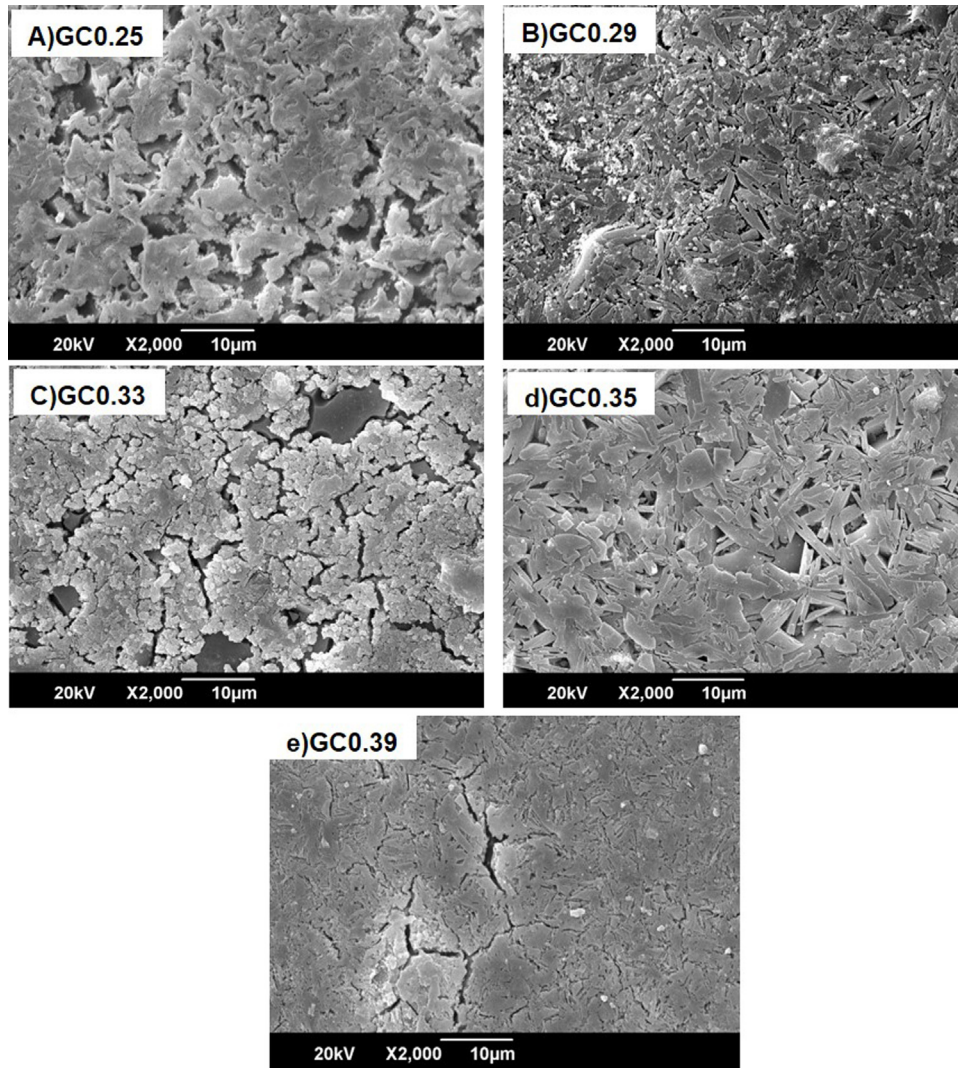
Fig. 8 – SEM images of the sintered samples.

observed in GC0.39; additionally, the size crystals is smaller compared with GC0.29 and GC0.35.

Physical and mechanical properties of glass–ceramics

Fig. 9 shows the variation of the bulk density and water absorption of the glass–ceramics obtained with respect to the SiO_2/Al_2O_3 molar ratio used to design the glasses (Table 2). In general, the bulk density of glass–ceramics is between 2607 ± 100 and $2739 \pm 60\,kg/m^3$; these values are similar to the reported bulk densities of wollastonite glass–ceramics [1]. The results presented in Fig. 9 show that higher densities are obtained in the glass–ceramic as there is a higher content of crystalline phases (GC0.29, GC0.39) (Fig. 7). Although this is not true for GC0.35. In general, these three samples showed less water absorption. The opposite is seen in samples of vitreous character, which correspond to those of greater molar ratio SiO_2/Al_2O_3 (Si/Al). In general, the results of water absorption (Fig. 9b) were between 0.13 ± 0.02 and $0.48 \pm 0.05\%$.

The Vickers microhardness values of the glass–ceramics GC0.29, GC0.33, GC0.35 and GC0.39 were of $643 \pm 29\,MPa$,

Table 4 – Mechanical properties determined by the nanoindentation test.

Sample	E (GPa)	H (GPa)	K_{ic} (MPa m$^{1/2}$)
GC0.29	96.20 ± 13.97	9.13 ± 1.48	0.46 ± 0.08
GC0.35	95.05 ± 5.33	9.34 ± 1.11	0.39 ± 0.03
GC0.39	96.12 ± 15.74	9.77 ± 1.67	0.59 ± 0.07

$570 \pm 14\,MPa$, $640 \pm 17\,MPa$ and $622 \pm 27\,MPa$ respectively. Yang [36] and Liu [38] found that increasing the CaO/SiO_2 ratio promotes glass crystallization. However, in this investigation the SiO_2/Al_2O_3 is an important parameter to control the crystallization process. Even samples with high CaO/SiO_2 and SiO_2/Al_2O_3 ratio such GC0.33 did not show ease of crystallization and mostly showed vitreous phase. Wollastonite-based glass–ceramics have usually, hardness values of $600\,MPa$ [1], but wollastonite was not observed in any of the studied mixtures.

The nanoindentation tests results for samples with higher crystal phases contents are shown in Table 4. The fracture toughness (K_{ic}) was determined by measuring the crack length
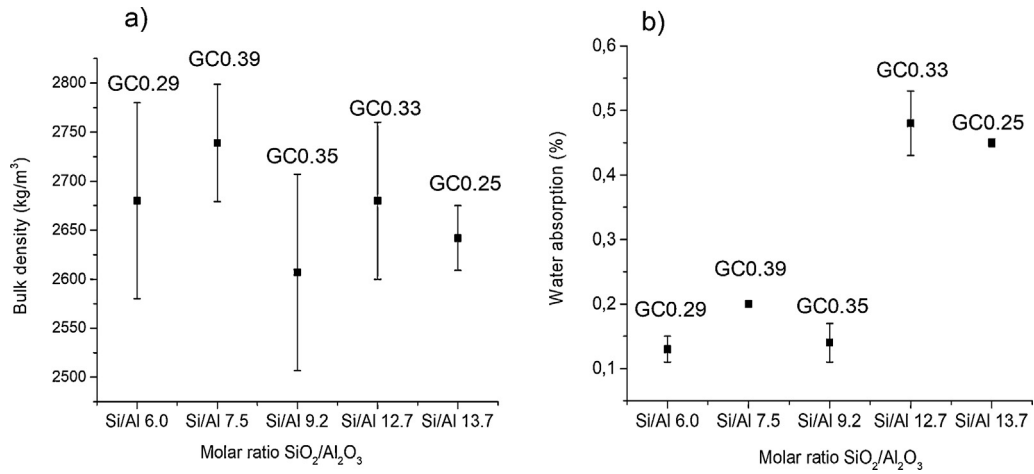
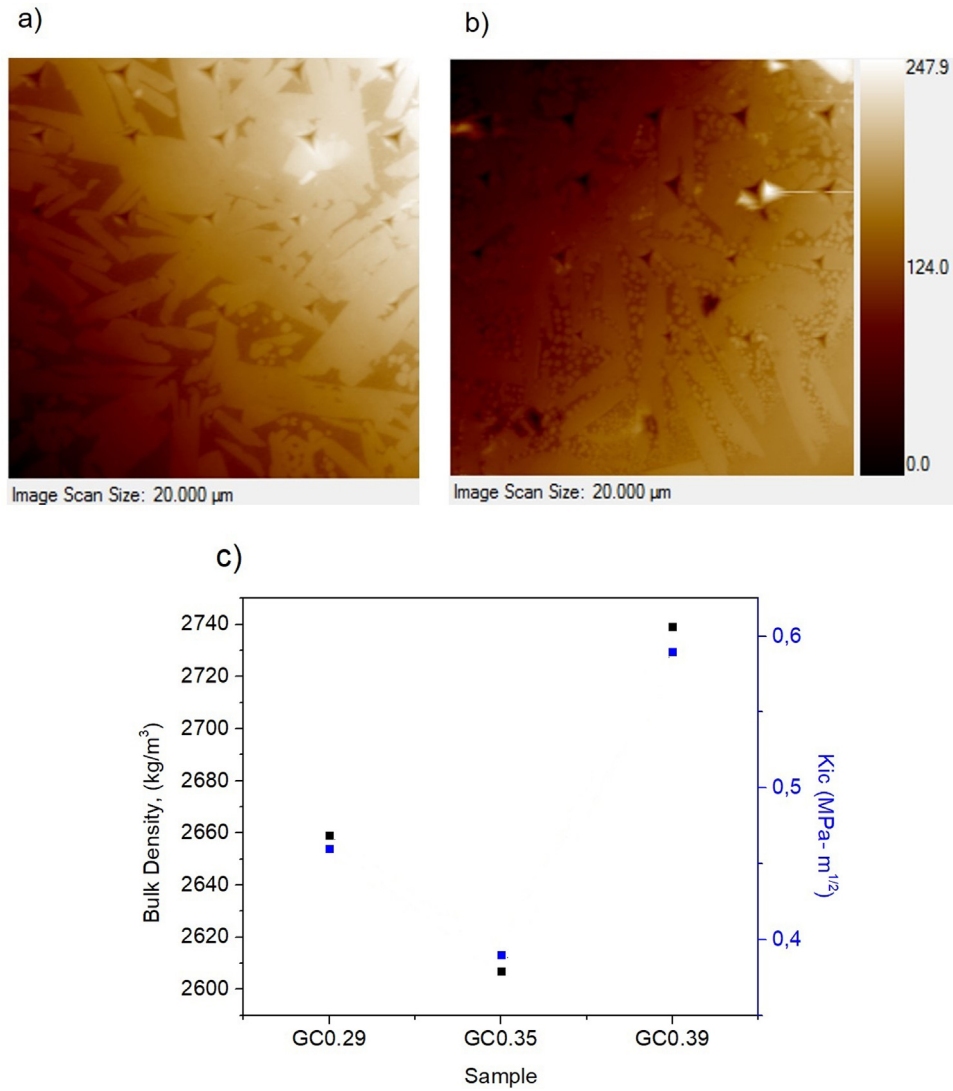Fig. 9 – (a) Bulk density and (b) water absorption of the glass–ceramics.

Fig. 10 – Images of the glass–ceramic samples, with marked locations of the indents on (a) GC0.39, (b) GC0.29 and (c) correlation between bulk density and K_{ic}.
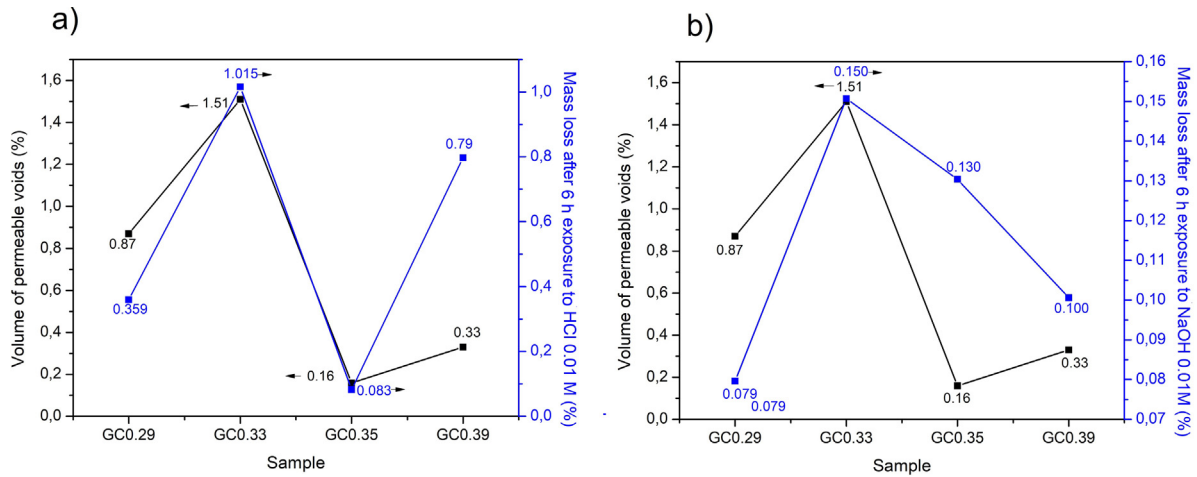
Fig. 11 – Volume of permeable voids in the glass–ceramics vs mass loss after 6 h exposures to 0.01 M HCl and NaOH solutions.

obtained in the Vickers hardness test, and the E was determined by the nanoindentation test. The K_{ic} was between 0.39 and 0.59 MPa m$^{1/2}$, and similar values were reported by Montoya-Quesada using fly ash [21]. Fig. 10a and b shows that although the Berkovich tip did not cause plastic deformation of the imprint, the imprints contain different phases, and the elastic modulus data obtained are homogenous. The hardness of the studied samples determined by nanoindentation (9.13–9.77 GPa) was higher relative to that reported for lithium silicate glasses (6.5 GPa) and their respective glass–ceramics (8.3 GPa) [34]. In general, the E was ∼96 GPa for the evaluated GC mixtures. Note that the SEM image of the glass–ceramics (Fig. 8) showed that these samples are partially crystallized, that is, they contain a residual glassy phase. In this regard, an elastic modulus of 133 GPa has been reported for fully crystalized glass–ceramic samples [34]. The E reported for the commercial glass–ceramic, Neopariés, is 86 GPa, whereas that of marble and natural granite is 75 GPa and 51 GPa, respectively [39], which indicates that the E of the glass–ceramics produced in this study was 10.6% higher than that of the commercial Neopariés glass–ceramic. An additional advantage is that the glass–ceramics produced in this work were obtained from industrial wastes such as CA and RHA. Fig. 10c shows the direct correlation between fracture toughness (K_{ic}) and the density of the glass–ceramics evaluated.

Durability in HCl and NaOH solutions

With respect to the application in construction the chemical durability is an important property of glass–ceramics, given that these materials are used as coatings, facades and elements that can be in contact with the environment. In acidic solutions, the hydrogen ions replace the alkaline ions in the glass structure, whereas in alkaline solutions, the silica structure is attacked [27]. Sample GC0.33 was the sample with the highest mass loss in the presence of HCl and NaOH and also contains the highest volume of permeable voids (Fig. 11a and b). This sample exhibited a lower proportion of crystalline phases, and as observed by the dynamic recrystallization test, the main phase was cristobalite.

Fig. 12 – Appearance of GC0.29 after immersion in HCl (left) and NaOH (right) solutions for 6 h.

The mass loss of the glass–ceramics GC0.29, GC0.33, GC0.35 and GC0.39 produced by acidic environment was 0.540, 0.503, 0.507 and 0.517 mg/cm^2, respectively. These mass losses are lower than the mass loss reported by Toya et al. [28], for glass–ceramics containing the anorthite and diopside phases and obtained from kaolin and dolomite wastes, 1.3 mg/cm^2. In the presence of NaOH, the mass losses of GC0.29, GC0.33, GC0.35 and GC0.39 were 0.529, 0.523, 0.484 and 0.522 mg/cm^2, respectively, which are also lower than the loss reported by Toya et al. (1.4 mg/cm^2) [28]. Lim et al. [40] reported mass losses above 30% for ceramics based on anorthite and exposed to acid solutions (10% HCl); in the present investigation, the mass loss values do not exceed 1.1% (Fig. 11a). The same authors report that in the presence of alkaline solutions (10% KOH), the mass loss was ∼0.43% after 5 h at 80 °C [40]; the glass–ceramics produced in this investigation (Fig. 11b) did not exceed a mass loss of 0.15%. Froberg et al. [27] found that the acid attack of the glass–ceramic samples containing the anorthite phase was relatively mild, since anorthite is formed in glasses with high corundum contents, and the glassy phase had a high alumina content, thus tending to increase the surface durability.

The reported mass losses of a commercial Neoparis glass–ceramic were 3.4 mg/cm^2 in acidic environments and

1.4 mg/cm^2 in alkaline environments [41]. Based on the results of previous investigations and the reported durability of commercial glass–ceramics, the glass–ceramics produced in this work are considered to have a high chemical durability. Fig. 12(left) demonstrates the change in color of the samples after immersion in HCl, showing some points of attack (pits) on the surface and a higher opacity and roughness. Over time, the material is expected to trap dust, lowering its cleaning capacity [42,43].

Conclusions

From the results here obtained, it can be concluded that was possible synthesizing glass–ceramics containing crystalline phases such as anorthite, albite and cristobalite from proper amounts of industrial wastes such as RHA and coal ash.

The CaO/SiO$_2$ ratio, as well as the SiO$_2$/Al$_2$O$_3$ ratio, contributes to the forming the crystalline phases. For this reason, samples with higher CaO/SiO$_2$ molar ratios but lower SiO$_2$/Al$_2$O$_3$ ratios result in anorthite and albite forming (GC0.29, GC0.35 and GC0.39). On the contrary, increasing the SiO$_2$/Al$_2$O$_3$ ratio (GC0.33) inhibits the crystallization of these phases, which significantly affects the final properties of the material.

The glass–ceramics obtained (GC0.29, GC0.35 and GC0.39) had densities between 2607 and 2739 kg/m^3 and a water absorption below 0.1%. The Vickers hardness was above 600 MPa, and the stiffness of the materials, determined by the nanoindentation test, was ∼96 GPa. The fracture toughness K_{ic} was between 0.39 and 0.59 MPa m$^{1/2}$. The chemical durability of these glass–ceramics exposed to HCl and NaOH was considered excellent (approximately 0.5 mg/cm^2), so they are good candidates for applications as construction materials, tiles, ceramic plates, coatings, among others.

Acknowledgments

REFERENCES

[1] W. Höland, G.H. Beall, Glass–Ceramic Technology, second ed., The American Ceramic Society, Westerville, 2012, http://dx.doi.org/10.1002/9781118265987.

[2] E.D. Zanotoo, A bright future for glass–ceramic, Am. Ceram. Soc. Bull. 89 (2010) 19–27.

[3] S. Zhang, Y. Zhang, T. Wu, Effect of Cr$_2$O$_3$ on the crystallization behavior of synthetic diopside and characterization of Cr-doped diopside glass ceramics, Ceram. Int. 44 (2018) 10119–10129, http://dx.doi.org/10.1016/j.ceramint.2018.02.231.

[4] R. Jia, L. Deng, F. Yun, H. Li, X. Zhang, X. Jia, Effects of SiO$_2$/CaO ratio on viscosity, structure, and mechanical properties of blast furnace slag glass ceramics, Mater. Chem. Phys. 233 (2019) 155–162, http://dx.doi.org/10.1016/j.matchemphys.2019.05.065.

[5] J.M. Klein, K.M.S. da Silva, A.P. Titton, R.C.D. Cruz, C.A. Perottoni, J.E. Zorzi, Microstructure and mechanical properties of a nucleant-free basaltic glass–ceramic, Mater. Sci. Technol. (United Kingdom) 35 (2019) 544–551, http://dx.doi.org/10.1080/02670836.2019.1572317.

[6] G.G. Santos, F.C. Serbena, V.M. Fokin, E.D. Zanotto, Microstructure and mechanical properties of nucleant-free Li$_2$O–CaO–SiO$_2$ glass–ceramics, Acta Mater. 130 (2017) 347–360, http://dx.doi.org/10.1016/j.actamat.2017.03.010.

[7] M.S. Dahiya, V.K. Tomer, S. Duhan, Bioactive Glass/Glass Ceramics for Dental Applications, Elsevier Inc., 2018, http://dx.doi.org/10.1016/b978-0-12-813742-0.00001-8.

[8] H. Bouchouicha, G. Panczer, D. de Ligny, Y. Guyot, R. Ternane, Luminescent properties of Eu-doped calcium aluminosilicate glass–ceramics: a potential tunable luminophore, Opt. Mater. (Amst.) 85 (2018) 41–47, http://dx.doi.org/10.1016/j.optmat.2018.08.006.

[9] V. Fuertes, J.F. Fernández, E. Enríquez, Enhanced luminescence in rare-earth-free fast-sintering glass–ceramic, Optica 6 (2019) 668, http://dx.doi.org/10.1364/optica.6.000668.

[10] L.A. Orlova, N.V. Popovich, N.E. Uvarova, A. Paleari, P.D. Sarkisov, High-temperature resistant glass–ceramics based on Sr-anorthite and tialite phases, Ceram. Int. 38 (2012) 6629–6634, http://dx.doi.org/10.1016/j.ceramint.2012.05.049.

[11] V. Fuertes, M.J. Cabrera, J. Seores, D. Muñoz, J.F. Fernández, E. Enríquez, Enhanced wear resistance of engineered glass–ceramic by nanostructured self-lubrication, Mater. Des. 168 (2019) 107623, http://dx.doi.org/10.1016/J.MATDES. 2019.107623.

[12] S. Chen, L.K. Liu, W. Li, Sintering behavior and dielectric properties of ultra-low temperature glass/ceramic composites, Mater. Res. Bull. 114 (2019) 107–111, http://dx.doi.org/10.1016/j.materresbull.2019.02.030.

[13] V. Fuertes, M.J. Cabrera, J. Seores, D. Muñoz, J.F. Fernández, E. Enríquez, Hierarchical micro-nanostructured albite-based glass–ceramic for high dielectric strength insulators, J. Eur. Ceram. Soc. 38 (2018) 2759–2766, http://dx.doi.org/10.1016/j.jeurceramsoc.2018.02.009.

[14] F.H. Margha, M.I. Badawy, T.A. Gad-Allah, ZnO enriched transparent glass–ceramics for wastewater decontamination, Environ. Prog. Sustain. Energy 36 (2017) 442–447, http://dx.doi.org/10.1002/ep.12482.

[15] D. Pan, L. Li, Y. Wu, T. Liu, H. Yu, Characteristics and properties of glass–ceramics using lead fuming slag, J. Clean. Prod. 175 (2018) 251–256, http://dx.doi.org/10.1016/j.jclepro.2017.12.030.

[16] C. Xi, F. Zheng, J. Xu, W. Yang, Y. Peng, Y. Li, P. Li, Q. Zhen, S. Bashir, J.L. Liu, Preparation of glass–ceramic foams using extracted titanium tailing and glass waste as raw materials, Constr. Build. Mater. 190 (2018) 896–909, http://dx.doi.org/10.1016/j.conbuildmat.2018.09.170.

[17] M. Zhu, R. Ji, Z. Li, H. Wang, L. Liu, Z. Zhang, Preparation of glass ceramic foams for thermal insulation applications from coal fly ash and waste glass, Constr. Build. Mater. 112 (2016) 398–405, http://dx.doi.org/10.1016/j.conbuildmat.2016.02.183.

[18] B. Karmakar, Functional glasses and glass–ceramics from solid waste materials, Funct. Glas. Glas. (2017) 295–315, http://dx.doi.org/10.1016/b978-0-12-805056-9.00009-x.

[19] V. Savvilotidou, A. Kritikaki, A. Stratakis, K. Komnitsas, E. Gidarakos, Energy efficient production of glass–ceramics using photovoltaic (P/V) glass and lignite fly ash, Waste Manag. 90 (2019) 46–58, http://dx.doi.org/10.1016/j.wasman.2019.04.022.

[20] H. Wang, Z. Chen, R. Ji, L. Liu, X. Wang, Integrated utilization of high alumina fly ash for synthesis of foam glass ceramic, Ceram. Int. 44 (2018) 13681–13688, http://dx.doi.org/10.1016/j.ceramint.2018.04.207.

[21] E. Montoya-Quesada, M.A. Villaquirán-Caicedo, R. Mejía de Gutiérrez, J. Muñoz-Saldaña, Effect of ZnO content on the physical, mechanical and chemical properties of glass–ceramics in the CaO–SiO_2–Al_2O_3 system, Ceram. Int. (2019), http://dx.doi.org/10.1016/j.ceramint.2019.10.154.

[22] J. Lu, Z. Zhang, Y. Li, Z. Liu, Effect of alumina source on the densification, phase evolution, and strengthening of sintered mullite-based ceramics from milled coal fly ash, Constr. Build. Mater. 229 (2019) 116851, http://dx.doi.org/10.1016/j.conbuildmat.2019.116851.

[23] M. Jordán, M.A. Montero, B. Rincón-Mora, J. Rincón, T. Sanfeliu, Rustic ceramic covering tiles obtained by recycling of marble residues and MSW fly ash, Fresen. Environ. Bull. 24 (2014) 533–538.

[24] F. Andreola, M.I. Martín, A.M. Ferrari, I. Lancellotti, F. Bondioli, J.M. Rincón, M. Romero, L. Barbieri, Technological properties of glass–ceramic tiles obtained using rice husk ash as silica precursor, Ceram. Int. 39 (2013) 5427–5435, http://dx.doi.org/10.1016/j.ceramint.2012.12.050.

[25] G. Sharma, S.K. Arya, K. Singh, Optical and thermal properties of glasses and glass–ceramics derived from agricultural wastes, Ceram. Int. 44 (2018) 947–952, http://dx.doi.org/10.1016/j.ceramint.2017.10.027.

[26] F. Naghizadeh, M.R. Abdul Kadir, A. Doostmohammadi, F. Roozbahani, N. Iqbal, M.M. Taheri, S.V. Naveen, T. Kamarul, Rice husk derived bioactive glass–ceramic as a functional bioceramic: synthesis, characterization and biological testing, J, Non Cryst. Solids 427 (2015) 54–61, http://dx.doi.org/10.1016/j.jnoncrysol.2015.07.017.

[27] L. Froberg, L. Hupa, M. Hupa, Corrosion of the crystalline phases of matte glazes in aqueous solutions, Eur. Ceram. Soc. 29 (2009) 7–14, http://dx.doi.org/10.1016/j.jeurceramsoc.2008.04.037.

[28] T. Toya, Y. Tamura, Y. Kameshima, K. Okada, Preparation and properties of CaO–MgO–Al_2O_3–SiO_2 glass–ceramics from kaolin clay refining waste (Kira) and dolomite, Ceram. Int. 30 (2004) 983–989, http://dx.doi.org/10.1016/J.CERAMINT.2003.11.005.

[29] J. Zhang, W. Dong, J. Li, L. Qiao, J. Zheng, J. Sheng, Utilization of coal fly ash in the glass–ceramic production, J. Hazard. Mater. 149 (2007) 523–526, http://dx.doi.org/10.1016/j.jhazmat.2007.07.044.

[30] I. Vereshchagin, Using quartzofeldspathic waste to obtain foamed glass material, Resour. Technol. 2 (2016) 23–29, http://dx.doi.org/10.1016/j.reffit.2016.05.001.

[31] A.R. Alao, L. Yin, Nano-mechanical behaviour of lithium metasilicate glass–ceramic, J. Mech. Behav. Biomed. Mater. 49 (2015) 162–174, http://dx.doi.org/10.1016/j.jmbbm.2015.05.002.

[32] J. Cheng, J. Xie, F. He, S. Yang, Stress analysis of CaO–Al_2O_3–SiO_2 system glass–ceramic with different thickness, J. Wuhan Univ. Technol. Mater. Sci. Ed. 20 (2005) 126–127, http://dx.doi.org/10.1007/BF02841303.

[33] G.R. Anstis, P. Chantikul, B.R. Lawn, D.B. Marshall, A critical evaluation of indentation techniques for measuring fracture toughness: I. Direct crack measurements, J. Am. Ceram. Soc. 64 (1981) 533–538.

[34] F.C. Serbena, I. Mathias, C.E. Foerster, E.D. Zanotto, Crystallization toughening of a model glass–ceramic, Acta Mater. 86 (2015) 216–228, http://dx.doi.org/10.1016/j.actamat.2014.12.007.

[35] V.O. Soares, J.K.M.B. Daguano, C.B. Lombello, O.S. Bianchin, L.M.G. Gonçalves, E.D. Zanotto, New sintered wollastonite glass–ceramic for biomedical applications, Ceram. Int. 44 (2018) 20019–20027, http://dx.doi.org/10.1016/j.ceramint.2018.07.275.

[36] Z. Yang, Q. Lin, S. Lu, Y. He, G. Liao, Y. Ke, Effect of CaO/SiO_2 ratio on the preparation and crystallization of glass–ceramics from copper slag, Ceram. Int. 40 (2014) 7297–7305, http://dx.doi.org/10.1016/j.ceramint.2013.12.071.

[37] L. Chunling, K. Sridhar, R. Rustum, Crystallization of anorthite-seeded albite glass by solid-state epitaxy, Am. Ceram. Soc. 75 (1992) 2665–2670, http://dx.doi.org/10.1111/j.1151-2916.1992.tb05486.x.

[38] Z.B. Liu, Y.B. Zong, H.Y. Ma, W.B. Dai, S.H. Li, Effect of $(CaO + MgO)/SiO_2$ ratio on crystallisation and properties of slag glass–ceramics, Adv. Appl. Ceram. 113 (2014) 411–418, http://dx.doi.org/10.1179/1743676114Y. 0000000187.

[39] Nippon, NEOPARIÉS Glass–Ceramic Building Materials, 2019, https://www.negb.co.jp/en/images/catalog/pdf/neoparies_en_catalog.pdf.

[40] W.B. Lim, D.W. Shin, B.C. Mohanty, Y.J. Park, Y.S. Cho, Chemical durability of anorthite-based low temperature co-fired ceramics, J. Ceram. Soc. Jpn. 117 (2009) 1138–1140, http://dx.doi.org/10.2109/jcersj2.117.1138.

[41] Z. Strand, Glass–Ceramic Materials: Glass Science Technology, vol. 8, 1986.

[42] T. Kronberg, L. Hupa, K. Fröberg, Durability of mat glazes in hydrochloric acid solution, Key Eng. Mater. 264–268 (2004) 1565–1568, http://dx.doi.org/10.4028/www.scientific.net/KEM.264-268.1565.

[43] L. Hupa, R. Bergman, L. Fröberg, S. Vane-Tempest, M. Hupa, T. Kronberg, E. Pesonen-Leinonen, A.-M. Sjöberg, Chemical resistance and cleanability of glazed surfaces, Surf. Sci. 584 (2005) 113–118, http://dx.doi.org/10.1016/J.SUSC.2004.11.048.